Journal of Alloys and Compounds 802 (2019) 573–582

Contents lists available at ScienceDirect

Journal of Alloys and Compounds

journal homepage: http://www.elsevier.com/locate/jalcom

Microstructure evolution and electroplasticity in Ti64 subjected to electropulsing-assisted laser shock peening

Hao Zhang [a], Zhencheng Ren [a], Jun Liu [a], Jingyi Zhao [a], Zhikun Liu [b], Dong Lin [c], Ruixia Zhang [a], Matthew J. Graber [a], Nicholas K. Thomas [a], Zachary D. Kerek [a], Guo-Xiang Wang [a], Yalin Dong [a, **], Chang Ye [a, *]

[a] Department of Mechanical Engineering, The University of Akron, Akron, OH, 44325, USA
[b] School of Mechanical Engineering, Shanghai Jiao Tong University, Shanghai, 200240, China
[c] Department of Industrial and Manufacturing Systems Engineering, Kansas State University, Manhattan, KS, 66506, USA

ARTICLE INFO

Article history:
Received 11 March 2019
Received in revised form
21 May 2019
Accepted 12 June 2019
Available online 13 June 2019

Keywords:
Electropulsing
Laser shock peening (LSP)
Electroplasticity
Resistive heating
Electron backscatter diffraction

ABSTRACT

In this study, an innovative surface treatment method, electropulsing assisted laser shock peening (EP-LSP), was used to process Ti64 samples. In EP-LSP, metallic samples are subjected to simultaneous high strain rate plastic deformation and high-frequency (100–500 Hz) short-duration (100 μs) pulsed electric current. The effects of EP-LSP on surface finish, microstructure, and micro-hardness of Ti64 alloy were investigated and compared with continuous current assisted LSP (CC-LSP) having the same bulk heating effect. It was observed that EP-LSP produced higher surface hardness and deeper hardened layer, both of which indicate greater plastic deformation. Tensile tests were carried out to evaluate the plasticity of Ti64 subjected to pulsed current and continuous current with the same bulk heating effect. It was observed that pulsed current can more effectively decrease the flow stress and thus resulted in greater plasticity in Ti64 compared with continuous current, even though the bulk heating effect was the same. In addition, the higher the peak current density, the more effective the flow stress reduction. As a result, pulsed current can more effectively improve the effectiveness of LSP treatment, as manifested by higher surface hardness and deeper plastic deformation layer. It is believed that an athermal effect in addition to the thermal effect related to pulsed current exists in EP-LSP.

1. Introduction

Laser shock peening (LSP) [1,2] can induce work-hardening and beneficial compressive residual stresses in the near-surface region of metallic components. Deep compressive residual stresses, grain refinement, and work hardening introduced by LSP could lead to significant improvement in wear resistance and fatigue resistance [3,4]. Since LSP is a surface engineering method based on plastic deformation, the low plasticity of the titanium alloy Ti64 makes it difficult to treat effectively using LSP. LSP with low laser intensity may not be sufficient to effectively generate beneficial changes in microstructure and residual stresses, while higher LSP intensity may damage the sample surface by inducing micro-cracks.

Electropulsing is a promising method that can improve the plasticity of metals previously subjected to deformation processing, including turning [5,6], rolling [7,8] and ultrasonic treatment [9–11;]. Deeper plastic-affected depth and finer grains were observed in Ti64 subjected to electropulsing-assisted ultrasonic surface modification [10]. In these studies, high-frequency (100–500 Hz) short-duration (50–200 μs) pulsed current was used to assist deformation processing. It was argued that pulsed electric current activates dislocation motion on non-basal planes of Ti64 and thus promotes more effective recrystallization when subjected to plastic deformation. The micro-hardness of Ti64 alloy was dramatically increased by the electropulsing-assisted ultrasonic surface rolling process [12]. In some cases, significant improvement in plasticity can be achieved while keeping the bulk temperature below 80 °C [13–15].

Even though electropulsing has been reported to significantly improve the efficiency of many deformation processes, the basic physics mechanisms of how pulsed current affects metal plasticity and thus the deformation process still merit further investigation. It

* Corresponding author.
** Corresponding author.
E-mail addresses: ydong@uakron.edu (Y. Dong), cye@uakron.edu (C. Ye).

https://doi.org/10.1016/j.jallcom.2019.06.156
0925-8388/

is not clear whether it is a pure thermal effect [16,17] or if there exists additional effects [18–20]. In some studies, it was suggested that the enhancement in plasticity is due entirely to Joule heating. For example, Magargee et al. [16] observed no flow stress reduction when forced air convection was used to maintain the sample at room temperature. Kinsey et al. [17] conducted electrically-assisted forming on Kolsky bars to evaluate the effect of electroplasticity at high strain rates (10^3 s^{-1}), and they found that the reduction is due entirely to Joule heating. However, it has also been reported that Joule heating alone cannot explain the dramatic change in microstructure and plasticity [20–26]. For example, Okazaki et al. [27] observed significant flow stress reduction in Ti subjected to pulsed current even when the sample was cooled to room temperature. A sudden decrease in flow stress was reported in aluminum alloys subjected to pulsed current during tensile testing [23]. As resistive heating is time-dependent, the immediate drop in flow stress cannot be explained by resistive heating alone. Perkins et al. [22] studied electrically assisted forging and found that the improvement in forgeability is significantly greater than what could be explained by bulk heating. Greater softening was observed in the sample with electrically-assisted heating than the sample that was oven-heated to the same bulk temperature. Zhao et al. [28] also found that pulsed current can more effectively reduce the flow stress of AZ31B magnesium alloy compared with a continuous current with the same bulk heating effect.

In addition to the dispute over whether or not the plasticity enhancement through pulsed current is a purely thermal effect, the advantages of pulsed current in comparison with continuous current in assisted deformation processing, if any, have yet to be studied. The aim of this study is to investigate the effect of electropulsing-assisted LSP (EP-LSP) on the microstructure evolution and improvement of mechanical properties of Ti64 alloy to explore the basic physics mechanism in metals subjected to simultaneous electropulsing and high strain rate plastic deformation. EP-LSP was used to treat Ti64 alloy, and its effects on surface finish, hardness, in-depth hardness, and microstructure evolution were investigated and compared with continuous current-assisted LSP (CC-LSP). To study whether the effect of pulsed current on the LSP process is purely thermal or not, the thermal effect from all sets of pulsed current and continuous current when using the same effective current density are compared. To understand how pulsed current affects metal plasticity and thus the EP-LSP process, tensile tests were carried out to evaluate the plasticity of Ti64 subjected to pulsed current and continuous current having the same thermal effect.

2. Experiments

2.1. Materials

Samples having dimensions of 10 mm × 10 mm × 0.8 mm were cut from a grade 5 titanium plate purchased from McMaster-Carr. The Ti64 plate has a nominal chemical composition of 5.50–6.75 wt% aluminum, 3.5–4.5 wt% vanadium, 0.4 wt% max. iron, 0.08 wt% carbon, 88.10–90.92 wt% titanium and 0–0.3% other components. The samples were abraded with silicon carbide sandpaper up to 1200 grit, followed by final polishing with a 1-μm diamond suspension. Mirror-like polished samples were cleaned in an ultrasonic cleaner using acetone, ethanol and deionized water in sequence prior to LSP, CC-LSP or EP-LSP treatment.

2.2. EP-LSP experiment

Fig. 1 presents a schematic of the EP-LSP process. All LSP experiments were carried out using a Continuum Surelite

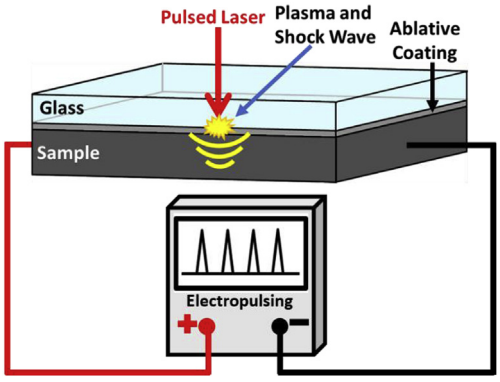

Fig. 1. Schematic of the EP-LSP process.

neodymium-doped yttrium aluminum garnet (Nd: YAG) laser with a wavelength of 1064 nm and a pulse duration (full width half maximum) of 5 ns. The laser intensity used was 4 GW/cm^2, the beam size was 1 mm, the frequency was 8 Hz, and the overlap was 75% in both the scanning and traverse directions. Nashua 322 multi-purpose foil tape with a thickness of 43 μm was used as the ablative coating. Borosilicate optical crown glass (BK7 transparent glass) with a thickness of 6.5 mm was used as the confinement media and was placed over the ablative material.

An in-house generator was used to provide a pulsed current with the appropriate electropulsing parameters (Table 1). The electropulsing parameters – which included peak current, frequency, pulse duration, and root-mean-square (RMS) current – were monitored using an oscilloscope. The current pulses were half sine-wave in form, and the pulse duration was 100 μs. The peak current and frequency were adjusted so that the same RMS current was used. The sample temperature during processing was monitored using a K-type thermocouple. For CC-LSP, the current density was adjusted to be the same as the RMS current in EP-LSP to keep the resistive heating effect constant. The electric current was applied to samples for 180 s before LSP to ensure that the temperature was stabilized.

2.3. Tensile tests

To evaluate the effect of pulsed current on the plasticity of Ti64, tensile tests were carried out. Dog-bone-shaped tensile samples with a gauge length of 10.5 mm, a width of 3.5 mm, a thickness of 0.83 mm, and a cross-sectional area of 2.905 mm^2 were cut from a plate using electrical discharge machining. The dimension of the tensile samples was designed according to the ASTM E8/E8M standard with the gauge length and gauge width scaled down proportionally. The power supply was connected to both ends of the tensile samples, and electric insulation was used between the

Table 1
Electrical parameters used in the CC-LSP and EP-LSP experiments.

Sample	Pulse frequency (Hz)	Peak current density (A/mm^2)	RMS current density (A/mm^2)
As-received	n/a	n/a	n/a
LSP	n/a	n/a	n/a
CC-LSP	n/a	13.7	13.7
EP-LSP-1	533	85.3	13.7
EP-LSP-2	256	109.7	13.7
EP-LSP-3	221	131.2	13.7
EP-LSP-4	200	145.1	13.7
EP-LSP-5	153	154.7	13.7

Table 2
Electrical parameters used during the tensile tests.

Sample	Pulse frequency (Hz)	Peak current density (A/mm^2)	RMS current density (A/mm^2)
CC-LSP	n/a	13.0	13.0
EP-LSP-1	750	65.4	12.1
EP-LSP-2	400	87.4	12.1
EP-LSP-3	240	113.6	12.1
EP-LSP-4	170	137.7	12.1
EP-LSP-5	140	165.2	12.1

tension clamps and the samples. A FLIR T650sc infrared (IR) camera was used to monitor the temperature of the samples during the tensile tests. Similar to the LSP experiments, an oscilloscope was used to monitor the frequency, peak current, pulse duration and RMS current. The RMS current densities were kept constant for all electropulsing-assisted tensile tests (at 12.1 A/mm^2) to ensure the heating effect of the electric current remained constant. The electropulsing parameters used in the tensile tests are given in Table 2. In tensile tests assisted by continuous current, to keep the bulk heating effect constant, the continuous current density was adjusted to 13.0 A/mm^2. The electric current was applied to samples 180 s before starting the tensile test to ensure that the temperature was stabilized. The tensile tests were conducted under a constant strain rate of 0.001 s^{-1}. Testing at each condition was repeated five times to ensure data reliability.

2.4. Surface morphology

A Zygo NewView 7300 surface profiler was used to characterize the surface roughness of the samples before and after LSP treatment. Two different magnifications were used: for a magnification of 25x, the scanning area was 2.83 mm by 2.12 mm; for a magnification of 100x, the scanning area was 0.71 mm by 0.53 mm.

2.5. Microstructure characterization

In order to investigate the microstructure after LSP, CC-LSP and EP-LSP, a number of characterization techniques were used.

2.5.1. Scanning electron microscopy

Cross sections of samples for scanning electron microscopy (SEM) examination were mechanically polished using 300-, 600-, 800- and 1200-grit silicon carbide sandpapers followed by a 1-μm polycrystalline diamond suspension. After polishing, all samples were cleaned using an ultrasonic cleaner in acetone, ethanol and deionized water in sequence and then etched with Kroll's reagent (2 ml of HF, 6 ml of HNO_3, and 92 ml of distilled water) prior to microstructural characterization using a Tescan Lyra 3 XMU scanning electron microscope.

2.5.2. Electron backscatter diffraction/orientation imaging microscopy

Cross sections of samples for electron backscatter diffraction (EBSD) and orientation imaging microscopy (OIM) examination were prepared by mechanical polishing to 1 μm, followed by finer polishing with 60 nm colloidal silica mixed with 10% hydrogen peroxide as an oxidizing agent for more than 10 h. EBSD scans with a step size of 90 nm were carried out using a Genesis 4040 EDAX/TSL EDS/EBSD system in a Tescan Lyra 3 XMU microscope operating at 20 kV.

2.5.3. Transmission electron microscopy

Transmission electron microscopy (TEM) samples were prepared using the focused ion beam (FIB) lift-out method in an FEI Helios Nanolab 650 SEM/FIB system in the Swagelok Center at Case Western Reserve University (Cleveland, Ohio). TEM observation was carried out using an FEI Tecnai F30 microscope operated at 300 kV.

2.6. Microhardness

The surface hardness and in-depth hardness of each Ti64 sample was characterized using a Wilson Tukon 1202 Vickers hardness testing system equipped with a diamond indenter. A holding duration of 10 s and a load of 50 g were used. In the results reported in this study, each surface hardness data point represents the average value of ten measurements. In-depth hardness was measured from the top surface to a depth of 100 μm on cross sections of the samples, and hardness values were collected at every 5 μm. Offsets in the horizontal direction were used to avoid indent overlapping.

3. Results

3.1. Surface hardness

Fig. 2a compares the surface hardness of the as-received Ti64 alloy subjected to LSP, CC-LSP and EP-LSP processing. LSP increased the surface microhardness by a marginal amount, about 1.1%, while CC-LSP treatment increased the surface hardness by 4.5%. Utilizing EP-LSP, the surface microhardness showed a considerable increase and improved by 13.4% for sample EP-LSP5. In addition, it can be observed from Fig. 2a that hardness increases with the peak current density for all EP-LSP cases, which indicates that increased peak current density could decrease the flow stress and generate greater

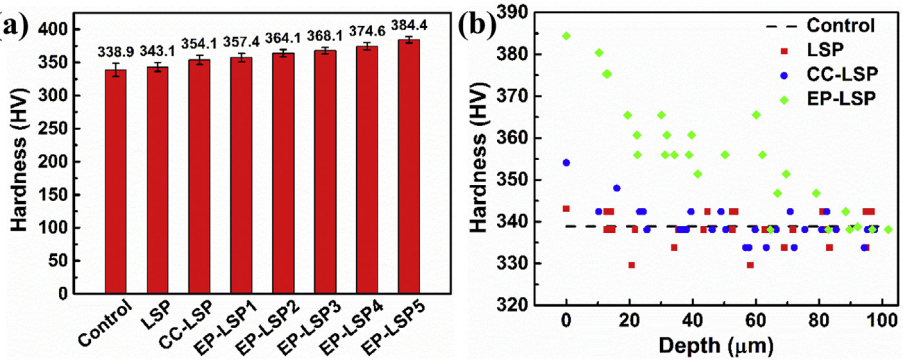

Fig. 2. (a) Surface hardness and (b) in-depth hardness for LSP, CC-LSP, and EP-LSP treatments.

plastic strain when the LSP intensity is constant (4 GW/cm^2). EP-LSP5 was identified as the optimal EP-LSP case and will be used for all future discussion. According to the in-depth hardness shown in Fig. 2b, EP-LSP also results in a deeper hardened layer compared with that for CC-LSP. The hardened layer for the EP-LSP sample has a thickness of 80 μm, while that for the CC-LSP sample is only about 25 μm. The lower flow stress is responsible for the deeper plastic-affected depth for the EP-LSP sample. Compared with CC-LSP, EP-LSP results in both higher surface hardness and deeper hardening layer even though the heating effect from electric current is the same. This means that the EP-LSP effects (i.e., higher surface hardness and deeper harden layer) cannot be fully explained by the thermal effect from resistive heating.

3.2. Surface roughness

Fig. 3 shows the surface roughness before and after different LSP treatments. It was found that the LSP-processed Ti64 samples maintained a similar level of roughness to that of the control samples, which indicates that LSP at room temperature did not introduce much plastic deformation to the sample surface. However, after CC-LSP and EP-LSP, the roughness of the samples increased significantly (from ~0.05 μm to ~0.30 μm), due to peening-induced indents and patterns. This indicates that both continous and pulse current could enhance the degree of plastic deformation induced by LSP.

3.3. X-ray diffraction

Fig. 4 shows the X-ray diffraction (XRD) patterns for Ti64 samples subjected to different treatments. The as-received material exhibited several α-Ti peaks and β-Ti peaks. A new peak at 44.8° with very low intensity was observed in the XRD patterns of CC-LSP and EP-LSP samples. It was not present in the control or the LSP samples. This low intensity peak indicates the possible presence of precipitates within the material after CC-LSP and EP-LSP treatment. This is consistent with the study by Liu et al. [29], in which they found that the application of continuous current to the ultrasonic surface modification process induced nanoscale precipitates in Ti64. Ye et al. [30,31] also found that warm laser shock peening could create high density nanoscale precipitates caused by dynamic strain aging and dynamic precipitation. The thermal energy added to the material increases the chemical driving force for precipitation. The local joule heating at defects likely assisted the precipitation process.

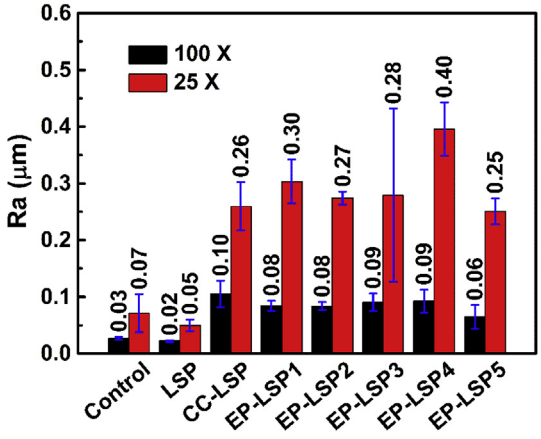

Fig. 3. Surface roughness at 25x and 100x magnifications after different treatments.

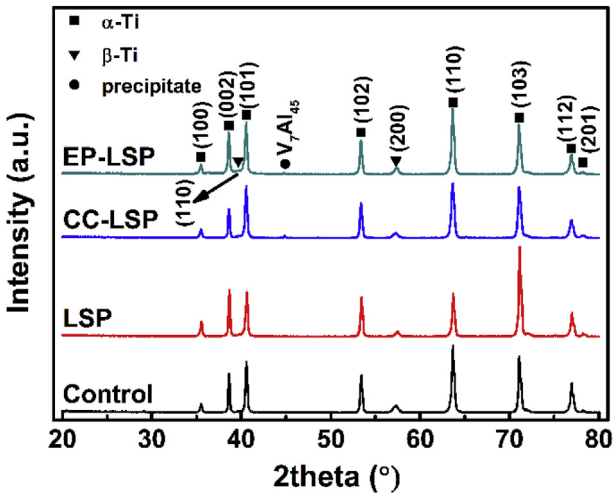

Fig. 4. XRD patterns of the Ti64 samples subjected to LSP, CC-LSP, and EP-LSP.

3.4. SEM

The cross-sectional microstructure of the Ti64 samples with different LSP treatments were observed and analyzed using SEM, as presented in Fig. 5. Typical microstructure of the cast Ti64 alloy can be observed with dark equiaxed α phase grains and light β phase embedded in the α phase grain boundaries. Note that no significant microstructure difference was observed from the SEM images for different LSP treatment. According to Lou et al. [32], only when the shock pressure generated by LSP is larger than the nanograin formation threshold or the critical driving force of deformation induced martensite can LSP induce significant microstructure evolution, such as grain refinement or phase transformation. Due to the plastic deformation induced by different LSP processes, a considerable number of dislocations and nano-twins were generated at the top layer of the processed alloy. EBSD and TEM were

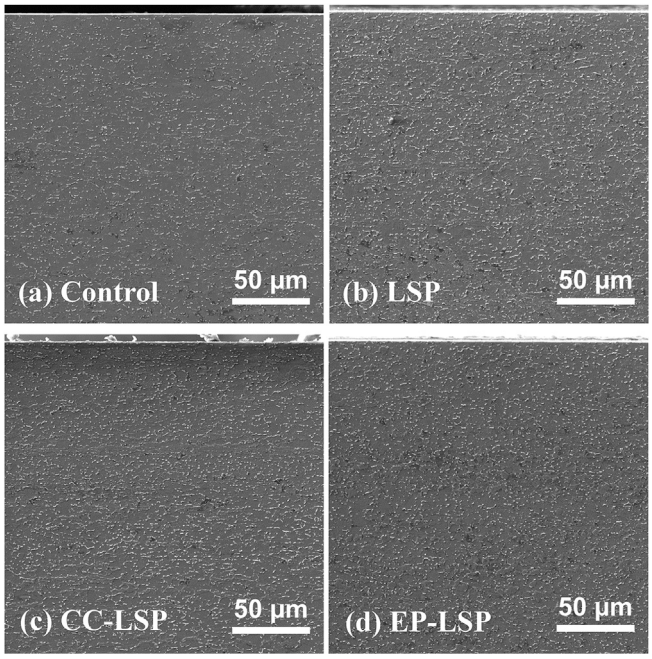

Fig. 5. Cross-sectional microstructure of Ti64 samples: (a) control, (b) LSP, (c) CC-LSP, and (d) EP-LSP.

used to further characterize the grain distortion and investigate the dislocation structures present in the samples that were not resolvable by SEM.

3.5. EBSD

Fig. 6a to f show the EBSD images and the kernel average misorientation (KAM) charts of Ti64 samples processed using different LSP treatments. Since no significant difference in grain size before and after different LSP treatments was observed in the EBSD images, the KAM method was used to evaluate the degree of plastic deformation. KAM is a measure of the average misorientation of a point with respect to a selected number of its nearest neighbors. A larger KAM value indicates a higher misorientation and, thus, a higher degree of plastic deformation. Fig. 6d, e and f show the KAM distribution of the LSP, CC-LSP and EP-LSP samples, respectively. It can be observed that the KAM values of both the CC-LSP and EP-LSP samples are higher than that of the LSP sample, with the EP-LSP sample having the highest KAM value (average KAM 1.125). Higher misorientation in the CC-LSP and EP-LSP samples indicates that more plastic strain was introduced through CC-LSP and EP-LSP, with the highest plastic strain generated by EP-LSP. Fig. 6g, h, and 6i show the KAM maps for the LSP, CC-LSP and EP-LSP samples, respectively. Higher and more uniform misorientation can be observed in the EP-LSP sample as compared with that in the CC-LSP sample, which is consistent with the KAM charts. This indicates that both continuous current and pulsed current can increase the plastic strain induced by LSP. In addition, it was found that pulsed

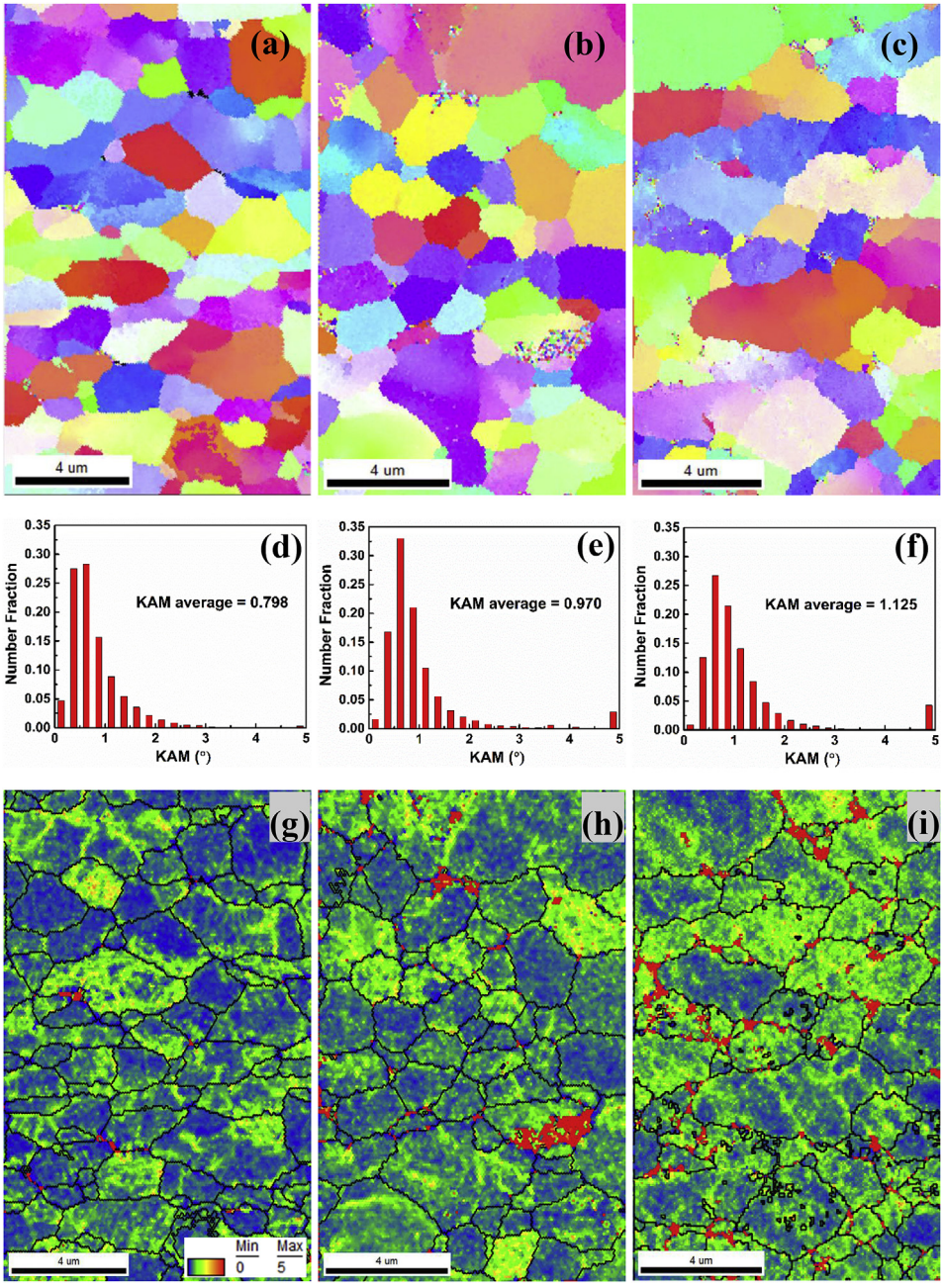

Fig. 6. Inverse pole figures (IPF) from EBSD observations in the cross sections of the samples (where all top edges correspond to the top surface of the samples) for (a) controls, (b) CC-LSP, (c) EP-LSP; KAM charts and maps corresponding to the (d, g) control, (e, h) CC-LSP, and (f, i) EP-LSP samples; the inset in (g) is the legend for all three KAM maps.

current is more effective in improving the processing effectiveness of LSP compared with continuous current having the same bulk heating effect.

To further study the effect of EP-LSP on surface texture as compared to CC-LSP, pole figures in the (0 0 0 1) α and (1 1 0) β directions were plotted in Fig. 7. The maximum intensities of different pole figures are listed in Table 3. It can be found for α phase, the maximum intensity of pole figure increases after CC-LSP and EP-LSP. The CC-LSP sample shows higher maximum intensity for the α phase than the EP-LSP sample. For the β phase, the maximum intensity of pole figure decreases after CC-LSP and EP-LSP processing, and EP-LSP induces the lowest maximum intensity in the β phase. It is known that plastic deformation introduced by LSP can locally change the initial texture in the top surface layer of Ti64 alloy, and the β phase, which has a body-centered cubic (BCC) crystal structure, can be more easily deformed as compared with the α phase, which has a hexagonal close packed (HCP) crystal structure. Thus, grain misorientation in the β phase is the main reason for the decrease in the maximum intensity. Lower maximum intensity of the β phase in the EP-LSP sample is attributed to the larger grain misorientation induced by EP-LSP than the misorientation induced by CC-LSP, which is also the reason for the lower maximum intensity of the α phase in the EP-LSP sample as compared with the CC-LSP sample. A similar result was reported for electropulsing-assisted ultrasonic surface rolling process [12]. As for the increase in maximum intensity of α phase after CC-LSP and EP-LSP, one possible reason is that the increase in maximum intensity induced by grain recovery and grain growth (at elevated temperatures by using an electric current) [33] is larger than the decrease in maximum intensity induced by grain distortion, which results from the low plasticity of the α phase present in the surfaces of these samples.

Table 3
Maximum intensity of different pole figures for Ti64 samples before and after different LSP treatments.

	Control	CC-LSP	EP-LSP
{0 0 0 1} α	11.399	17.182	13.430
{1 1 0} β	10.766	5.026	4.485

3.6. TEM

The TEM images of the top surface layers of Ti64 samples processed using LSP and EP-LSP are shown in Fig. 8. Dislocation walls and dislocation tangles can be observed in both samples. Limited deformation features such as dislocations and twin boundaries are observed (Fig. 8b and c) in the LSP-processed sample, while some bending contours exist at the top layer (as indicated by the red arrow in Fig. 8a) due to the TEM sample preparation. The generation of such multi-directional mechanical twins (MTs), which can be seen in Fig. 8c, is in good accordance with that observed in pure titanium subjected to multiple rounds of LSP processing [34]. The low density for the dislocations and twin boundaries indicates that the degree of plastic deformation is quite low in the LSP-processed sample. Because the stacking fault energy of the α phase is lower than that of the β phase, twins can be easily formed in the α phase of the Ti64 alloy [35]. In contrast, in the images in Fig. 8g–i, a higher density of dislocations was observed in the EP-LSP sample. Not only can planer dislocations [36] be observed in the image shown in Fig. 8g, but also dense dislocation tangles; dislocation walls and dislocation cells can be observed in the images in Fig. 8e and f. The increased dislocation activity might be caused by the higher dislocation mobility as a result of electropulsing [37–41]. Once the twins are no longer able to accommodate the plastic strain, dense dislocations are generated near grain boundaries and twin boundaries, which have higher strain and easily act as dislocation nucleation sites. In addition, similar to the observations of Lainé et al. [36], sub-grain boundaries formed from complex arrays of dislocations can be observed in Fig. 8i, which reveal the higher distortion inside the grains of the EP-LSP sample as compared with that of the LSP sample. This finding is consistent with the EBSD results and further confirms that electropulsing can enhance the degree of plastic deformation when the LSP intensity is the same.

4. Discussion

The effect of peak current density is investigated by processing the samples using the same RMS current density with different peak current densities. By using the same RMS current density, the temperature profiles during EP-LSP treatment for all EP-LSP samples should be the same, as shown in Fig. 9. According to Fig. 9, it can be seen that the sample temperatures reached during CC-LSP

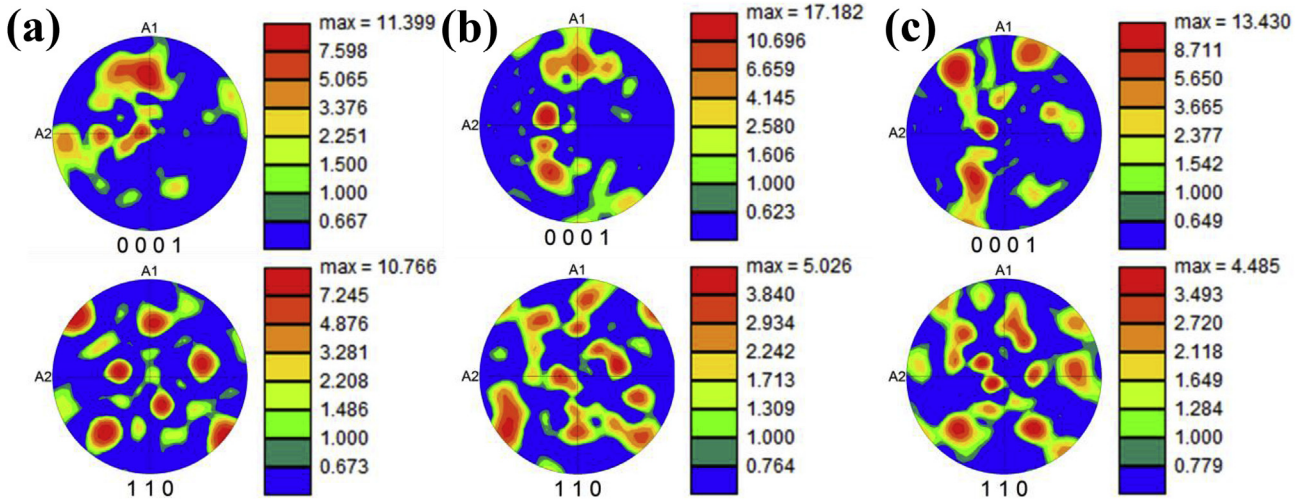

Fig. 7. Pole figures from EBSD observation of the cross sections (where all top edges correspond to the top surface of the samples) of the (a) control, (b) CC-LSP, and (c) EP-LSP samples.

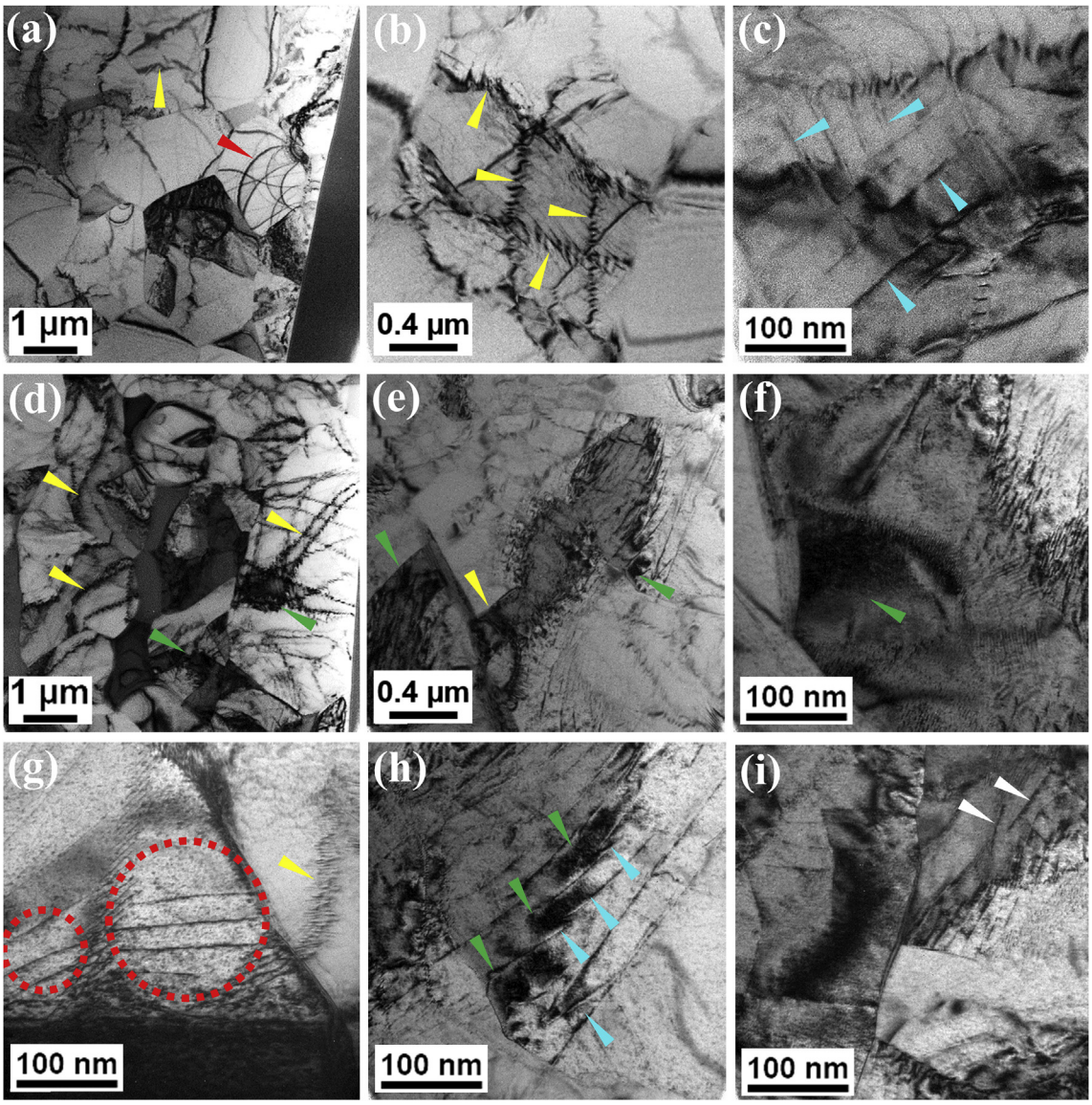

Fig. 8. Bright-field TEM micrographs of near-surface microstructures of LSP (a–c) and EP-LSP-processed (d–i) Ti64 samples. In these images, bending contours are indicated by red arrows, dislocation walls are indicated by yellow arrows, twin boundaries are indicated by cyan arrows, dislocation tangles are indicated by green arrows, planar dislocations are enclosed in red-dashed circles, and sub-grain boundaries are indicated by white arrows. (For interpretation of the references to colour in this figure legend, the reader is referred to the Web version of this article.)

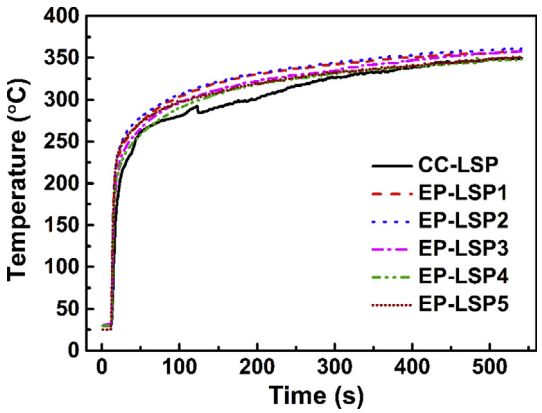

Fig. 9. Temperature history for samples processed using CC-LSP and EP-LSP.

treatment and the various EP-LSP treatments are from 25 °C to around 361 °C, and the maximum temperatures for the different treatments range between 350 °C and 361 °C. Very close heating rates, temperature histories, and maximum temperatures are reasonable, as the same RMS current density was applied in all treatments. Thus, the thermal effects for the different treatments should be the same. However, according to the above results, while the thermal effect is the same, the hardening effect varies according to the current type and peak current density used in the treatment. These phenomena indicate that the effect of EP-LSP, once the peak current density exceeds a critical value, goes beyond the thermal effect.

It is found that when the peak current increases, the surface hardness of the EP-LSP processed sample increases gradually. As the temperature is the same for all samples, the thermal contribution to surface hardness increase should also be the same, which would indicate that the peak current density is responsible for the

higher hardness of the EP-LSP samples. It is possible that pulsed current with a higher peak current density can more effectively lower the flow stress and thus induce more significant strain hardening that leads to higher hardness. Note that sample EP-LSP1 has a similar hardening effect as compared to the sample subjected to CC-LSP treatment (Fig. 2). This suggests that when the peak current is lower than a critical value, the surface hardness will be close to the hardness of the samples processed with continuous current using the same RMS current. It also indicates that when the peak current density is not high enough, its contribution is purely thermal.

In order to investigate the effect of pulsed current and continuous current on the plasticity of the Ti64 alloy, a series of tensile tests were performed. During the tensile tests, the RMS current densities for electropulsing were kept the same for all tensile tests (12.1 A/mm^2) to ensure the heating effect of the electric current would remain the same (Fig. 10a). The peak current densities for the electropulsing varied from 65.4 A/mm^2 to 165.2 A/mm^2 to study the effect of peak current density, and the frequency was adjusted to maintain a constant RMS current density. A continuous current with the same RMS current density (12.1 A/mm^2) was also used. However, using a continuous current with an RMS of 12.1 A/mm^2 resulted in a lower temperature than that in the five samples processed using pulsed current. The lower temperature of the continuous current sample could result from the lower dynamic electric resistivity for continuous current than that for pulsed current according to the Drude model. In order to maintain a consistent thermal effect, the CC current density was adjusted to 13.0 A/mm^2. Fig. 10b shows the engineering strain–stress curves of Ti64 samples under different peak current densities with same RMS current density for all EP sets. It was observed that pulsed current can more effectively decrease the flow stress of Ti64 compared with continuous current, even though the bulk heating effect is the same. When plotting the tensile strength as a function of the peak current density in Fig. 10c, it is interesting to note that the tensile stress decreases almost linearly with the peak current density. Lower flow stress indicates higher plasticity and higher dislocation mobility. Even though the RMS current densities are the same (and thus the thermal effect), higher peak current density can more effectively increase dislocation mobility and thus more effectively decrease the flow stress, which is beneficial for deformation-based manufacturing processes. This observation is consistent with a previous study, in which pulsed current was observed to induce significantly higher plasticity in AZ31B compared with continuous current [28].

Flow stress is the instantaneous stress required to continue plastically deform the material and to keep the metal flowing. It is known that plastic deformation in metals is accomplished predominantly through dislocation movement. Electric current is considered to be able to reduce the stress needed to generate dislocations from dislocation sources, such as the grain boundary and pre-existing dislocations [38,42,43]. It was reported that EP can induce localized high dislocation concentration around the obstacles and thus dissociate the immobile dislocation junctions in a single-crystalline $Ge_2Sb_2Te_5$ through *in-situ* TEM [42]. In addition, the effect of pulsed current on dislocation mobility also affects the plasticity. According to the studies by Gromov et al. [37,38], pulsed electric current can increase the dislocation velocity, and higher current density leads to higher dislocation velocity under the same resolved shear stress and temperature. Since a large number of crystal defects (e.g. grain boundaries, precipitates and dislocation tangles) are pre-existing or are being generated during plastic deformation, localized Joule heating from electron-defect scattering [44] could be significant during the EP-LSP process. Higher energy absorption at crystal defects can reduce the resistance for dislocations to slip through obstacles like precipitates and grain boundaries [45–48]. Based on the results in this study, by controlling the effective current density and varying the peak current

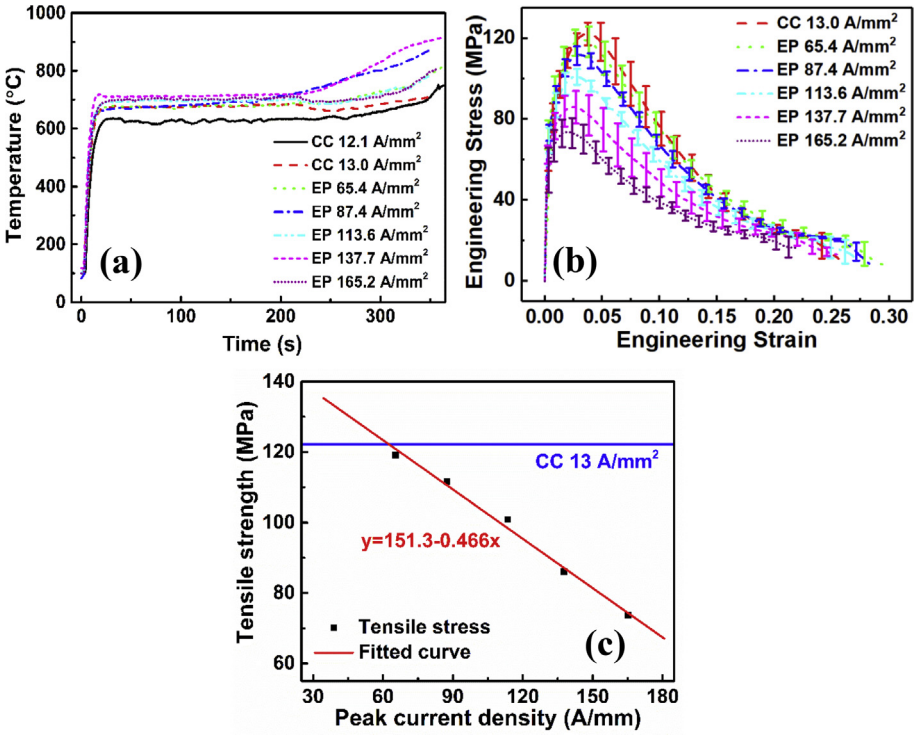

Fig. 10. (a) The temperature profile and (b) strain–stress curves of Ti64 samples subjected to continuous and pulsed current, and (c) the tensile strength as a function of the peak current density.

density, it is found that a pulsed current with high peak current density can more effectively lower the flow stress and can thus improve the effectiveness of LSP treatment even though the thermal effect is the same. It is believed that when the effective current density is the same, higher peak current density can more effectively mobilize the dislocations and thus decrease the flow stress [28], which results in greater work-hardening and thus higher hardness. It is thus believed that pulsed current with a sufficiently high peak current density is more efficient for increasing the effectiveness of LSP compared with a continuous current having the same heating effect.

5. Conclusion

In this study, an innovative surface engineering process called EP-LSP was studied for the first time. It was observed that EP-LSP results in higher surface hardness and a deeper hardened layer compared with CC-LSP having the same thermal effect. This means that the effect of pulsed current on the LSP process goes beyond the thermal effect. In addition, it was found that the effectiveness of EP-LSP increases with peak current density when the effective current density is constant. Tensile testing was carried out to study the effect of pulsed current on the plasticity of Ti64. It was found that pulsed current can more effectively lower the flow stress of Ti64 compared with continuous current having the same heating effect. In addition, the degree of flow stress reduction increases with the peak current density even though the effective current density and thus the thermal heating effect are the same. It is believed that compared with continuous current, pulsed current with much higher peak current density can more effectively lower the flow stress and thus results in greater degree of work-hardening, which leads to greater surface hardness of deeper hardened layer in EP-LSP. This study has demonstrated that the effect of pulsed current on the plasticity of Ti64 goes beyond the thermal effect. In addition, the EP-LSP effect cannot be fully explained by resistive heating alone. Even though more in-depth study is needed to reveal the fundamental mechanisms of EP-LSP, this study serves as a first attempt to utilize high-frequency short-duration pulsed current to increase the effectiveness of LSP, or any other deformation-based manufacturing processes, without requiring a significant increase in sample temperature.

Acknowledgments

The authors are grateful for the financial support of this research by the NSF CAREER program (CMMI 1847247).

References

[1] J. Zhao, Y. Dong, C. Ye, Laser shock peening induced residual stresses and the effect on crack propagation behavior, Int. J. Fatigue 100 (2017) 407–417, https://doi.org/10.1016/j.ijfatigue.2017.04.002.
[2] J.Z. Lu, K.Y. Luo, Y.K. Zhang, G.F. Sun, Y.Y. Gu, J.Z. Zhou, X.D. Ren, X.C. Zhang, L.F. Zhang, K.M. Chen, C.Y. Cui, Y.F. Jiang, A.X. Feng, L. Zhang, Grain refinement mechanism of multiple laser shock processing impacts on ANSI 304 stainless steel, Acta Mater. 58 (2010) 5354–5362, https://doi.org/10.1016/j.actamat.2010.06.010.
[3] J.Z. Lu, K.Y. Luo, Y.K. Zhang, C.Y. Cui, G.F. Sun, J.Z. Zhou, L. Zhang, J. You, K.M. Chen, J.W. Zhong, Grain refinement of LY2 aluminum alloy induced by ultra-high plastic strain during multiple laser shock processing impacts, Acta Mater. 58 (2010) 3984–3994, https://doi.org/10.1016/j.actamat.2010.03.026.
[4] P. Peyre, R. Fabbro, L. Berthe, X. Scherpereel, E. Bartnicki, Laser-shock processing of materials and related measurements, in: C.R. Phipps (Ed.), High-Power Laser Ablation, 1998, pp. 183–193, https://doi.org/10.1117/12.321565.
[5] A.J. Sánchez Egea, H.A. González Rojas, C.A. Montilla Montaña, V. Kallewaard Echeverri, Effect of electroplastic cutting on the manufacturing process and surface properties, J. Mater. Process. Technol. 222 (2015) 327–334, https://doi.org/10.1016/j.jmatprotec.2015.03.018.
[6] H. Wang, L. Chen, D. Liu, G. Song, G. Tang, Study on electropulsing assisted turning process for AISI 304 stainless steel, Mater. Sci. Technol. 00 (2015), https://doi.org/10.1179/1743284715Y.0000000034, 1743284715Y.000.
[7] H. Liao, G. Tang, Y. Jiang, Q. Xu, S. Sun, J. Liu, Effect of thermo-electropulsing rolling on mechanical properties and microstructure of AZ31 magnesium alloy, Mater. Sci. Eng. A 529 (2011) 138–142, https://doi.org/10.1016/j.msea.2011.09.007.
[8] J. Kuang, X. Li, R. Zhang, Y. Ye, A.A. Luo, G. Tang, Enhanced rollability of Mg-3Al-1Zn alloy by pulsed electric current: a comparative study, Mater. Des. 100 (2016) 204–216, https://doi.org/10.1016/j.matdes.2016.03.126.
[9] D. Liu, X. Li, G. Tang, L. Chen, H. Wang, G. Song, Improvement of surface properties of 2316 stainless steel with ultrasonic electric surface modification, Mater. Sci. Technol. 00 (2015), https://doi.org/10.1179/1743284715Y.0000000042, 1743284715Y.000.
[10] Y. Ye, H. Wang, G. Tang, G. Song, Effect of electropulsing-assisted ultrasonic nanocrystalline surface modification on the surface mechanical properties and microstructure of Ti-6Al-4V alloy, J. Mater. Eng. Perform. 27 (2018) 2394–2403, https://doi.org/10.1007/s11665-018-3248-3.
[11] Y. Ye, X. Li, J. Kuang, Y. Geng, G. Tang, Effects of electropulsing assisted ultrasonic impact treatment on welded components, Mater. Sci. Technol. 00 (2015), https://doi.org/10.1179/1743284715Y.0000000078, 1743284715Y.000.
[12] H. Wang, G. Song, G. Tang, Evolution of surface mechanical properties and microstructure of Ti 6Al 4V alloy induced by electropulsing-assisted ultrasonic surface rolling process, J. Alloy. Comp. 681 (2016) 146–156, https://doi.org/10.1016/j.jallcom.2016.04.067.
[13] Y.H. Zhu, S. To, W.B. Lee, X.M. Liu, Y.B. Jiang, G.Y. Tang, Effects of dynamic electropulsing on microstructure and elongation of a Zn–Al alloy, Mater. Sci. Eng. A 501 (2009) 125–132, https://doi.org/10.1016/j.msea.2008.09.080.
[14] Q. Xu, L. Guan, Y. Jiang, G. Tang, S. Wang, Improved plasticity of Mg–Al–Zn alloy by electropulsing tension, Mater. Lett. 64 (2010) 1085–1087, https://doi.org/10.1016/j.matlet.2010.02.017.
[15] Q. Xu, G. Tang, Y. Jiang, G. Hu, Y. Zhu, Accumulation and annihilation effects of electropulsing on dynamic recrystallization in magnesium alloy, Mater. Sci. Eng. A 528 (2011) 3249–3252, https://doi.org/10.1016/j.msea.2010.12.101.
[16] J. Magargee, F. Morestin, J. Cao, Characterization of flow stress for commercially pure titanium subjected to electrically assisted deformation, J. Eng. Mater. Technol. 135 (2013) 041003, https://doi.org/10.1115/1.4024394.
[17] B. Kinsey, G. Cullen, A. Jordan, S. Mates, Investigation of electroplastic effect at high deformation rates for 304SS and Ti–6Al–4V, CIRP Ann 62 (2013) 279–282, https://doi.org/10.1016/j.cirp.2013.03.058.
[18] M.I. Molotskii, Theoretical basis for electro- and magnetoplasticity, Mater. Sci. Eng. A 287 (2000) 248–258, https://doi.org/10.1016/S0921-5093(00)00782-6.
[19] H. Conrad, Electroplasticity in metals and ceramics, Mater. Sci. Eng. A 287 (2000) 276–287, https://doi.org/10.1016/S0921-5093(00)00786-3.
[20] C.D. Ross, T.J. Kronenberger, J.T. Roth, Effect of dc on the formability of Ti–6Al–4V, J. Eng. Mater. Technol. 131 (2009) 031004, https://doi.org/10.1115/1.3078307.
[21] M.S. Siopis, B.L. Kinsey, Experimental investigation of grain and specimen size effects during electrical-assisted forming, J. Manuf. Sci. Eng. 132 (2010) 021004, https://doi.org/10.1115/1.4001039.
[22] T.A. Perkins, T.J. Kronenberger, J.T. Roth, Metallic forging using electrical flow as an alternative to warm/hot working, J. Manuf. Sci. Eng. 129 (2007) 84, https://doi.org/10.1115/1.2386164.
[23] W.A. Salandro, J.J. Jones, T. McNeal, A.J.T. Roth, S.-T. Hong, M.T. Smith, Formability of Al 5xxx sheet metals using pulsed current for various heat treatments, J. Manuf. Sci. Eng. 132 (2010) 051016, https://doi.org/10.1115/1.4002185.
[24] C.M. Dzialo, M.S. Siopis, B.L. Kinsey, K.J. Weinmann, Effect of current density and zinc content during electrical-assisted forming of copper alloys, CIRP Ann 59 (2010) 299–302, https://doi.org/10.1016/j.cirp.2010.03.014.
[25] M.S. Siopis, B.L. Kinsey, N. Kota, O.B. Ozdoganlar, Effect of severe prior deformation on electrical-assisted compression of copper specimens, J. Manuf. Sci. Eng. 133 (2011) 064502, https://doi.org/10.1115/1.4005351.
[26] J.T. Roth, I. Loker, D. Mauck, M. Warner, S.F. Golovashchenko, A. Krause, Enhanced formability of 5754 aluminum sheet metal using electric pulsing, Trans. North Am. Manuf. Res. Inst. SME 36 (2008) 405–412.
[27] K. Okazaki, M. Kagawa, H. Conrad, A study of the electroplastic effect in metals, Scripta Metall. 12 (1978) 1063–1068, https://doi.org/10.1016/0036-9748(78)90026-1.
[28] J. Zhao, Z. Ren, H. Zhang, G.-X. Wang, Y. Dong, C. Ye, Electroplasticity in AZ31B subjected to short-duration high-frequency pulsed current, J. Appl. Phys. 125 (2019) 185104, https://doi.org/10.1063/1.5087465.
[29] J. Liu, S. Suslov, S. Li, H. Qin, Z. Ren, G.L. Doll, H. Cong, Y. Dong, C. Ye, Electrically assisted ultrasonic nanocrystal surface modification of Ti6Al4V alloy, Adv. Eng. Mater. 20 (2018) 1700470, https://doi.org/10.1002/adem.201700470.
[30] C. Ye, S. Suslov, B.J. Kim, E.A. Stach, G.J. Cheng, Fatigue performance improvement in AISI 4140 steel by dynamic strain aging and dynamic precipitation during warm laser shock peening, Acta Mater. 59 (2011) 1014–1025, https://doi.org/10.1016/j.actamat.2010.10.032.
[31] C. Ye, Y. Liao, S. Suslov, D. Lin, G.J. Cheng, Ultrahigh dense and gradient nanoprecipitates generated by warm laser shock peening for combination of high strength and ductility, Mater. Sci. Eng. A 609 (2014) 195–203, https://doi.org/10.1016/j.msea.2014.05.003.
[32] S. Lou, Y. Li, L. Zhou, X. Nie, G. He, Y. Li, W. He, Surface nanocrystallization of metallic alloys with different stacking fault energy induced by laser shock processing, Mater. Des. 104 (2016) 320–326, https://doi.org/10.1016/j.matdes.2016.05.028.

[33] Y.J. Liu, Z. Liu, Y. Jiang, G.W. Wang, Y. Yang, L.C. Zhang, Gradient in microstructure and mechanical property of selective laser melted AlSi10Mg, J. Alloy. Comp. 735 (2018) 1414–1421, https://doi.org/10.1016/j.jallcom.2017.11.020.
[34] J.Z. Lu, L.J. Wu, G.F. Sun, K.Y. Luo, Y.K. Zhang, J. Cai, C.Y. Cui, X.M. Luo, Microstructural response and grain refinement mechanism of commercially pure titanium subjected to multiple laser shock peening impacts, Acta Mater. 127 (2017) 252–266, https://doi.org/10.1016/j.actamat.2017.01.050.
[35] X.D. Ren, W.F. Zhou, F.F. Liu, Y.P. Ren, S.Q. Yuan, N.F. Ren, S.D. Xu, T. Yang, Microstructure evolution and grain refinement of Ti-6Al-4V alloy by laser shock processing, Appl. Surf. Sci. 363 (2016) 44–49, https://doi.org/10.1016/j.apsusc.2015.11.192.
[36] S.J. Lainé, K.M. Knowles, P.J. Doorbar, R.D. Cutts, D. Rugg, Microstructural characterisation of metallic shot peened and laser shock peened Ti–6Al–4V, Acta Mater. 123 (2017) 350–361, https://doi.org/10.1016/j.actamat.2016.10.044.
[37] V.E. Gromov, L.I. Gurevich, V.F. Kurilov, T.V. Erilova, Influence of current pulses on the mobility and multiplication of dislocations in Zn, Strength Mater. 21 (1989) 1335–1341, https://doi.org/10.1007/BF01529261.
[38] V.E. Gromov, L.I. Gurevich, V.A. Kuznetsov, T. V Erilova, Influence of electric current pulses on the mobility and multiplication of dislocations in Zn-monocrystals, Czech. J. Phys. 40 (1990) 895–902, https://doi.org/10.1007/BF01597960.
[39] H. Conrad, J. White, W.D. Cao, X.P. Lu, A.F. Sprecher, Effect of electric current pulses on fatigue characteristics of polycrystalline copper, Mater. Sci. Eng. A 145 (1991) 1–12, https://doi.org/10.1016/0921-5093(91)90290-4.
[40] A.F. Sprecher, S.L. Mannan, H. Conrad, Overview no. 49: on the mechanisms for the electroplastic effect in metals, Acta Metall. 34 (1986) 1145–1162, https://doi.org/10.1016/0001-6160(86)90001-5.
[41] K. Okazaki, M. Kagawa, H. Conrad, A study of the electroplastic effect in metals, Scripta Metall. 12 (1978) 1063–1068, https://doi.org/10.1016/0036-9748(78)90026-1.
[42] S.-W. Nam, H.-S. Chung, Y.C. Lo, L. Qi, J. Li, Y. Lu, A.T.C. Johnson, Y. Jung, P. Nukala, R. Agarwal, Electrical wind force-driven and dislocation-templated amorphization in phase-change nanowires, Science 336 (2012) 1561–1566, https://doi.org/10.1126/science.1220119, 80-.
[43] Y.-H. Liao, C.-L. Liang, K.-L. Lin, A.T. Wu, High dislocation density of tin induced by electric current, AIP Adv. 5 (2015) 127210, https://doi.org/10.1063/1.4937909.
[44] J. Zhao, G.-X. Wang, Y. Dong, C. Ye, Multiscale modeling of localized resistive heating in nanocrystalline metals subjected to electropulsing, J. Appl. Phys. 122 (2017) 085101, https://doi.org/10.1063/1.4998938.
[45] K. Chen, N. Tamura, B.C. Valek, K.N. Tu, Plastic deformation in Al (Cu) interconnects stressed by electromigration and studied by synchrotron polychromatic x-ray microdiffraction, J. Appl. Phys. 104 (2008) 013513, https://doi.org/10.1063/1.2952073.
[46] A.S. Budiman, C.S. Hau-Riege, W.C. Baek, C. Lor, A. Huang, H.S. Kim, G. Neubauer, J. Pak, P.R. Besser, W.D. Nix, Electromigration-induced plastic deformation in Cu interconnects: effects on current density exponent, n, and implications for EM reliability assessment, J. Electron. Mater. 39 (2010) 2483–2488, https://doi.org/10.1007/s11664-010-1356-4.
[47] A. Rahnama, R. Qin, Room temperature texturing of austenite/ferrite steel by electropulsing, Sci. Rep. 7 (2017) 42732, https://doi.org/10.1038/srep42732.
[48] H. Shen, W. Zhu, Y. Li, N. Tamura, K. Chen, In situ synchrotron study of electromigration induced grain rotations in Sn solder joints, Sci. Rep. 6 (2016) 24418, https://doi.org/10.1038/srep24418.